

## Understanding the electronic properties of carbon polyprismanes from the $sp^3$ tight-binding model

Vladimir A. Kurakin<sup>1</sup>, Tatyana N. Kobernik<sup>2</sup><sup>1</sup>National Research Nuclear University MEPhI, Moscow, Russia<sup>2</sup>Energy Technology Center, Skolkovo Institute of Science and Technology, Moscow, RussiaCorresponding author: Vladimir A. Kurakin, [fromkurakin@mail.ru](mailto:fromkurakin@mail.ru)

**ABSTRACT** Carbon polyprismanes are 1D nanostructures that should be classified as diamond-like phases because they (polyprismanes) also consist of the 4-coordinated carbon atoms. A carbon polyprismane contains polygonal atomic rings arranged in layers along the common symmetry axis, at uniform distances from each other. According to previous density functional theory based studies, carbon polyprismanes can exhibit metallic conductivity, which is very unusual for diamond-like phases. In this paper, we present the  $sp^3$  tight-binding model based calculations of the band structures for carbon polyprismanes of different diameters and compare the obtained results with their analogs for a 2D square carbon lattice, which can be considered as the limiting case of a carbon polyprismane of infinite diameter. Our results confirm that the  $sp^3$  tight-binding model describes the electronic properties of carbon polyprismanes well, since we obtain their band structures over a wide range of parameter values for the proposed model. We believe that such electronic transport characteristics are an intrinsic topological feature of polyprismanes and should also occur in non-carbon polyprismanes.

**KEYWORDS** band structure, tight-binding model, polyprismane, carbon nanostructures

**FOR CITATION** Kurakin V.A., Kobernik T.N. Understanding the electronic properties of carbon polyprismanes from the  $sp^3$  tight-binding model. *Nanosystems: Phys. Chem. Math.*, 2025, **16** (2), 209–215.

### 1. Introduction

In recent years, carbon nanotubes (CNTs) have found increasingly diverse applications in nanotechnology, engineering, and industry. CNTs are actively used in the fabrication of various electronic components such as ionic diodes [1], electrodes [2], and field-effect transistors (FETs) [3–5]. Many of the modern advances in CNT-based electronics have evolved from devices employing a single CNT to implementations using aligned CNTs and even CNT thin films, as demonstrated in [6]. Aligned CNT-based field-effect transistors have already been scaled down to sizes below 10 nm, surpassing their silicon counterparts in terms of charge carrier mobility and the Fermi velocity [7]. Moreover, artificial synaptic thin-film transistors, fabricated on an ultrathin flexible substrate with semiconductor single-walled CNTs (SWCNTs) exhibiting high charge carrier mobility, have proved useful for the development of neuromorphic electronic skin [8]. In addition, CNTs have helped researchers fabricate highly conductive polymer composites for rapid-response electrical heaters [9] and even electroactive porous filters for water purification [10].

A notable feature of CNTs is that their carbon atoms are in an  $sp^2$ -hybridized state and can form additional covalent bonds. Consequently, CNTs tend to be quite sensitive to environmental contaminants (free radicals). Carbon polyprismanes (CPPs), or  $C_{[n,m]}$  prismanes – systems of regular atomic  $m$ -gons stacked in layers along a common symmetry axis at uniform inter-layer distances ( $n$  is the number of such  $m$ -gons; see Fig. 1) – do not suffer from this disadvantage because the atoms in such CPPs are in an  $sp^3$ -hybridized state and cannot form any additional covalent bonds. CPPs also have much smaller cross-sectional areas compared to SWCNTs. These two factors make  $C_{[n,m]}$  prismanes particularly attractive in certain high-tech applications requiring atomic-scale precision (e.g., in the fabrication of ultrathin nanoneedles for biological applications or tips for atomic force microscopy [11]).

However, CPPs are not without their drawbacks, one of which is low thermal stability. Thus far, only the simplest  $C_{[n,m]}$  prismanes have been synthesized [12–14]. Nevertheless, we believe that even these CPPs can be very useful in nanoelectronics. It is well known that scaling down FET contact lengths is challenging as it can degrade device performance [15]. Some studies report significant deterioration of FETs at their contact lengths below 30 nm [16]. We believe that even the simplest  $C_{[n,m]}$  prismanes could be promising candidates for nanomaterials to help solve these scaling issues.

In addition, computational modeling indicates that long ( $n \geq 10$  or even  $n \rightarrow \infty$ )  $C_{[n,4]}$ ,  $C_{[n,5]}$ , and  $C_{[n,6]}$  prismanes are sufficiently stable [17, 18], and also predicts the feasibility of creating  $C_{[3,4]}$  and  $C_{[4,4]}$  prismanes [19]. Direct molecular-dynamics simulations confirm the high kinetic stability of short  $C_{[2,6]}$  and  $C_{[2,8]}$  prismanes [20]. Density functional theory (DFT) calculations have also been applied to study specific CPP-based electronic components, such as Schottky nanodiodes [21].

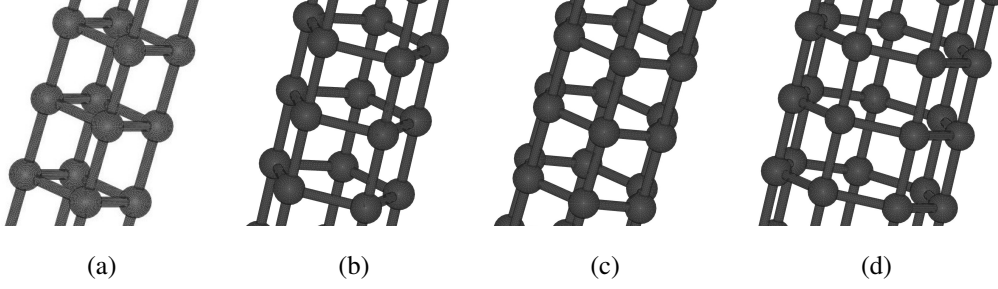


FIG. 1. Atomic structures of  $C_{[n,4]}$  (a),  $C_{[n,5]}$  (b),  $C_{[n,6]}$  (c), and  $C_{[n,7]}$  (d) prismanes

Many diamond-like phases are very robust and can withstand substantial mechanical loads, as demonstrated by atomistic modeling [22–24]. Some diamond-like phases have hardness values comparable to that of diamond [25]. Such distinctive physical properties open a broad range of commercial applications for diamond-like phases. Furthermore, like diamond, most diamond-like phases comprise fully  $sp^3$ -bonded carbon atoms and often have sizable ( $> 3.0$  eV) band gaps (diamond’s band gap is about 5.45 eV [26]), i.e., they display dielectric behavior [27]. Although  $C_{[n,m]}$  prismanes are structural units of diamond-like phases, CPPs can exhibit metallic conductivity, which is highly unusual for  $sp^3$ -hybridized carbon materials. This has been shown via DFT-based studies [28, 29]. Notably, analogous metallic properties also appear in silicon and germanium (classical semiconductors) polyprismanes [30–32], suggesting that the electrical transport characteristics of  $C_{[n,m]}$  prismanes are driven by their topology rather than by carbon’s intrinsic nature.

The tight-binding model (TBM) is a relatively simple and intuitive approach to calculating the band structures of both carbon [33, 34] and non-carbon [35–37] materials. In this paper, we understand the metallic conductivity of CPPs from the  $sp^3$  tight-binding model ( $sp^3$ -TBM).

## 2. Materials and methods

We applied the  $sp^3$ -TBM to compute the band structures of sufficiently long  $C_{[n,m]}$  prismanes ( $n \rightarrow \infty$ ,  $m = 4, 5, 6, 7$ ). The  $2s$ ,  $2p_x$ ,  $2p_y$ , and  $2p_z$  orbitals of each carbon atom were used as the basis set for expressing this model. The Bloch functions used in our proposed model can be described as follows:

$$|\psi_\lambda(\mathbf{k}, \boldsymbol{\rho})\rangle = -\frac{1}{\sqrt{N_0}} \sum_{i=1}^{N_0} e^{-i(\mathbf{k} \cdot \mathbf{a}_i)} |\phi_\lambda(\boldsymbol{\rho} - \mathbf{a}_i - \boldsymbol{\tau}_\eta)\rangle,$$

where the index  $\lambda$  runs over the  $2s$ ,  $2p_x$ ,  $2p_y$ , and  $2p_z$  atomic orbitals,  $l$  is the number of CPP unit cell,  $\mathbf{a}_l$  is the translation vector of the  $l$ -th unit cell along the  $C_{[n,m]}$  prismane symmetry axis,  $\boldsymbol{\tau}_\eta$  is the relative displacement of the  $\eta$ -th atom in the unit cell of this CPP,  $\mathbf{k}$  is the wave vector (directed along the CPP symmetry axis and lying in the 1st Brillouin zone),  $N_0$  is the total number of CPP unit cells ( $N_0 = n \rightarrow \infty$ ),  $\boldsymbol{\rho}$  is the electron radius-vector. The general form of the  $m \times m$  Hamiltonian sub-block for a long  $C_{[n,m]}$  prismane in the basis set  $|\phi_\lambda(\boldsymbol{\rho} - \mathbf{a}_i - \boldsymbol{\tau}_\eta)\rangle$  is detailed in Table 1, where it is assumed that the  $q$ -th atom is the nearest neighbor of the  $p$ -th atom, and the  $r$ -th atom is the nearest neighbor of the  $q$ -th atom but not of the  $p$ -th atom.

TABLE 1. General form of the  $m \times m$  Hamiltonian sub-block

Atom index	$p$ -th atom	$q$ -th atom	$r$ -th atom
$p$ -th atom	$E$	$-e^{-i(\mathbf{k} \cdot \mathbf{d}_{p,q})} E_{p,q}$	0
$q$ -th atom	$-e^{-i(\mathbf{k} \cdot \mathbf{d}_{q,p})} E_{q,p}$	$E$	$-e^{-i(\mathbf{k} \cdot \mathbf{d}_{q,r})} E_{q,r}$
$r$ -th atom	0	$-e^{-i(\mathbf{k} \cdot \mathbf{d}_{r,q})} E_{r,q}$	$E$

In Table 1, the elements  $E$ ,  $E_{q,p}$ ,  $E_{p,q}$ ,  $E_{q,r}$ , and  $E_{r,q}$  are  $4 \times 4$  matrices describing the interaction energies of the long  $C_{[n,m]}$  prismane atoms with indices  $p$ ,  $q$ , and  $r$ . The vector  $\mathbf{d}_{i,j}$  represents the position of atom  $j$  of such a CPP relative to its atom  $i$ . The matrices  $E_{q,p}$ ,  $E_{p,q}$ ,  $E_{q,r}$ , and  $E_{r,q}$  were calculated according to the Slater–Koster approach (see Table 2) [38]. We likewise computed the elements  $E$ , taking into account that each atom in the  $C_{[n,m]}$  prismane ( $n \rightarrow \infty$ ) unit cell interacts with its 2 images in the nearest neighboring unit cells of this CPP. The matrices  $E$  also included the energies of the  $s$ - and  $p$ -orbitals of carbon. Since we only considered the interactions of the nearest neighboring atoms of CPPs, ( $p$ ;  $r$ ) and ( $r$ ;  $p$ ) blocks in Table 1 are 0.

In Table 2,  $L$ ,  $M$ , and  $N$  are the direction cosines of  $\mathbf{d}_{i,j}$  with respect to  $x$ -,  $y$ -, and  $z$ -axes, respectively. Throughout this work, we assumed that all covalent bond-lengths in  $C_{[n,m]}$  prismanes ( $n \rightarrow \infty$ ) are equal ( $\sim 1.50 - 1.60$  Å),

TABLE 2. Elements of the matrices  $E_{q,p}$ ,  $E_{p,q}$ ,  $E_{q,r}$ , and  $E_{r,q}$ 

Atomic orbitals	$2s$	$2p_x$	$2p_y$	$2p_z$
$2s$	$t_{ss\sigma}$	$Lt_{sp\sigma}$	$Mt_{sp\sigma}$	$Nt_{sp\sigma}$
$2p_x$	$Lt_{sp\sigma}$	$L^2t_{pp\sigma} + (1 - L^2)t_{pp\pi}$	$LM(t_{pp\sigma} - t_{pp\pi})$	$LN(t_{pp\sigma} - t_{pp\pi})$
$2p_y$	$Mt_{sp\sigma}$	$LM(t_{pp\sigma} - t_{pp\pi})$	$M^2t_{pp\sigma} + (1 - M^2)t_{pp\pi}$	$NM(t_{pp\sigma} - t_{pp\pi})$
$2p_z$	$Nt_{sp\sigma}$	$LN(t_{pp\sigma} - t_{pp\pi})$	$NM(t_{pp\sigma} - t_{pp\pi})$	$N^2t_{pp\sigma} + (1 - N^2)t_{pp\pi}$

as previous studies indicate that in long CPPs the difference between intra-layer and inter-layer bond-lengths does not exceed 5 % [11]. Thus, our focus was on elucidating the electronic properties of long  $C_{[n,m]}$  prismanes rather than on fine details of their geometry. In explaining the electrical transport characteristics of such CPPs, we adopted the simplest possible model.

All eigenvalue calculations of the Hamiltonians and the band structure plots were performed numerically using Python.

### 3. Results and discussion

In the first phase of our study, we adopted the following parameter values for the  $sp^3$ -TBM:  $E_{2s} = -7.30$ ,  $E_{2p} = 0.00$ ,  $t_{ss\sigma} = -4.30$ ,  $t_{sp\sigma} = 4.98$ ,  $t_{pp\sigma} = 6.38$ , and  $t_{pp\pi} = -2.66$  eV, as indicated in [39–41].

Before calculating the band structures of  $C_{[n,m]}$  prismanes ( $n \rightarrow \infty$ ,  $m = 4, 5, 6, 7$ ) with these  $sp^3$ -TBM parameter values, we tested them by computing the band structures of long zigzag  $(\chi, 0)$  SWCNTs. For  $\chi = 6, 7, 8, 9$  our results qualitatively confirmed the well-known rule: if  $\chi$  is a multiple of 3, then long  $(\chi, 0)$  SWCNTs are quasi-metallic [42]. Fig. 2 shows the band structures of long  $(6, 0)$ ,  $(7, 0)$ ,  $(8, 0)$ , and  $(9, 0)$  SWCNTs under the chosen parameter values for the  $sp^3$ -TBM. The corresponding band gaps of these SWCNTs are summarized in Table 3.

TABLE 3. Band gaps of long  $(\chi, 0)$  SWCNTs

$\chi$	6	7	8	9
Band gap, eV	0.08	1.14	1.11	0.08

We initially validated the above  $sp^3$ -TBM parameter values on  $(\chi, 0)$  SWCNTs because they are 1D systems (like CPPs). In addition, the electric transport characteristics of such SWCNTs are fairly well understood. However, each carbon atom in long SWCNTs has only three nearest neighbors. In long  $C_{[n,m]}$  prismanes, each carbon atom is covalently bonded to its four nearest neighbors. Therefore, we additionally tested the same  $sp^3$ -TBM parameter values by reproducing the electronic properties of diamond, which indeed demonstrated a distinct dielectric character under these conditions.

Using the above parameter values for the  $sp^3$ -TBM, we then calculated the band structures of long  $[n, 4]$ ,  $[n, 5]$ ,  $[n, 6]$ , and  $[n, 7]$  CPPs. Our results indicate that  $C_{[n,m]}$  prismanes begin to exhibit metallic properties for  $m \geq 5$ , whereas  $C_{[n,4]}$  prismanes display a pronounced dielectric character ( $n \rightarrow \infty$ ). These findings for long  $C_{[n,4]}$  and  $C_{[n,m]}$  prismanes with  $m \geq 7$  are in qualitative agreement with the DFT-based calculations in [29]. Fig. 3 shows the band structures of long  $C_{[n,4]}$ ,  $C_{[n,5]}$ ,  $C_{[n,6]}$ , and  $C_{[n,7]}$  prismanes under the chosen parameter values for the  $sp^3$ -TBM. The corresponding band gaps of these CPPs are provided in Table 4.

TABLE 4. Band gaps of  $[n, m]$  CPPs at  $n \rightarrow \infty$ 

$m$	4	5	6	7
Band gap, eV	5.48	0.00	0.00	0.00

The accuracy of both TBM- and DFT-based calculations depends on the choice of parameter values and other approximations [43–46]. Consequently, in the second phase of our work, we varied each of the  $sp^3$ -TBM parameter values by  $\pm 30$  % of their respective initial values and evaluated the effect of these variations on the electronic properties of long  $[n, 4]$ ,  $[n, 5]$ ,  $[n, 6]$ , and  $[n, 7]$  CPPs. The band gaps of  $C_{[n,4]}$  and  $C_{[n,m]}$  prismanes with  $m \geq 7$  and  $n \rightarrow \infty$  proved to be qualitatively stable under these changes. In contrast, the band gaps for long  $[n, 5]$  and  $[n, 6]$  CPPs ranged from 0.00 to 1.00 eV under the similar shifts of the parameter values for the  $sp^3$ -TBM, indicating a quasi-metallic to semiconducting behavior of such CPPs, in agreement with [29]. The persistence of the qualitative results for the band gaps of long  $C_{[n,4]}$

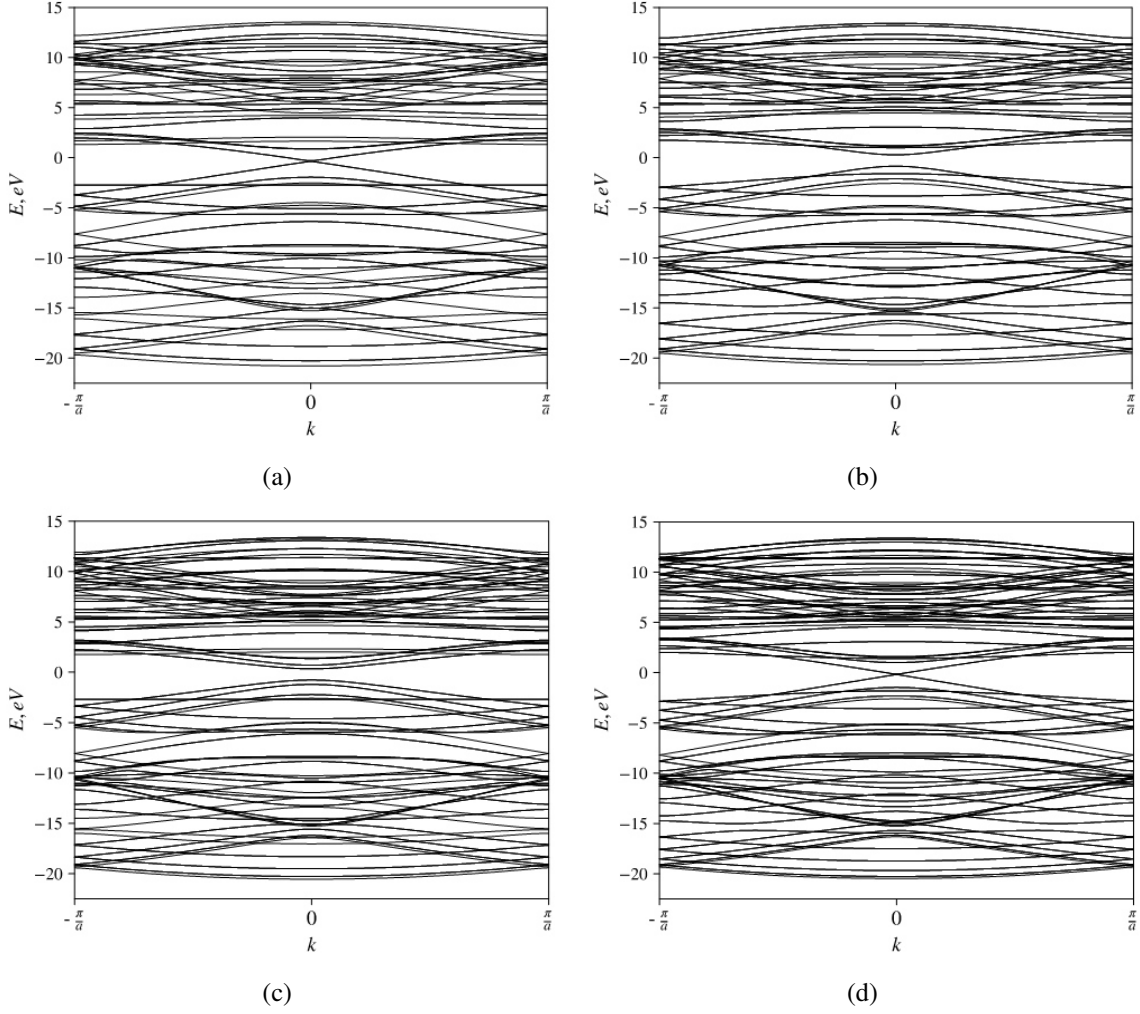


FIG. 2. Band structures of long (6, 0) (a), (7, 0) (b), (8, 0) (c), and (9, 0) (d) SWCNTs

and  $C_{[n,m]}$  prismanes ( $m \geq 7$ ) suggests that their electric transport characteristics are mainly due to the topology of these CPPs and are not very sensitive to specific  $sp^3$ -TBM parameter values. Table 5 compiles the resulting intervals of the band gaps for long  $[n, 4]$ ,  $[n, 5]$ ,  $[n, 6]$ , and  $[n, 7]$  CPPs under the above variations of  $sp^3$ -TBM parameter values.

TABLE 5. Band gap intervals for long  $[n, m]$  CPPs under a variation of the  $sp^3$ -TBM parameter values ( $E_{2s}$ ,  $E_{2p}$ ,  $t_{ss\sigma}$ ,  $t_{sp\sigma}$ ,  $t_{pp\sigma}$ ,  $t_{pp\pi}$ )

$m$	4	5	6	7
Band gap intervals, eV	2.12 – 10.18	0.00 – 0.93	0.00 – 0.80	0.00 – 0.00

It is well known that the band gap of a long  $(\chi, 0)$  SWCNT decreases with increasing its diameter, and such a SWCNT itself herewith tends asymptotically towards graphene [42]. Similarly, a long  $C_{[n,m]}$  prismane with very large diameter ( $m \rightarrow \infty$ ) asymptotically approaches a hypothetical infinite 2D square carbon lattice (Fig. 4(a)). Although in a long  $C_{[n,m]}$  prismane the intra-layer atomic distances differ slightly from their inter-layer analogs, this discrepancy diminishes for larger diameter of this CPP [11]. As the surface curvature of a long CPP approaches 0 and all its covalent bond-lengths become equal, the structure of such a  $C_{[n,m]}$  prismane essentially becomes to a hypothetical infinite 2D square carbon lattice. Although this ideal lattice is likely to be unstable in practice, it is instructive to consider it as the limiting case of a long CPP with a very large diameter. Fig. 4(b) shows the band structure of a hypothetical infinite 2D square carbon lattice calculated with the above  $sp^3$ -TBM parameter values. Varying these parameter values did not have a qualitative impact on the outcome: for  $C_{[n,m]}$  prismanes in the limits  $n \rightarrow \infty$  and  $m \rightarrow \infty$ , the band gap remains zero, indicating robust metallic conduction of the ideal carbon lattice.

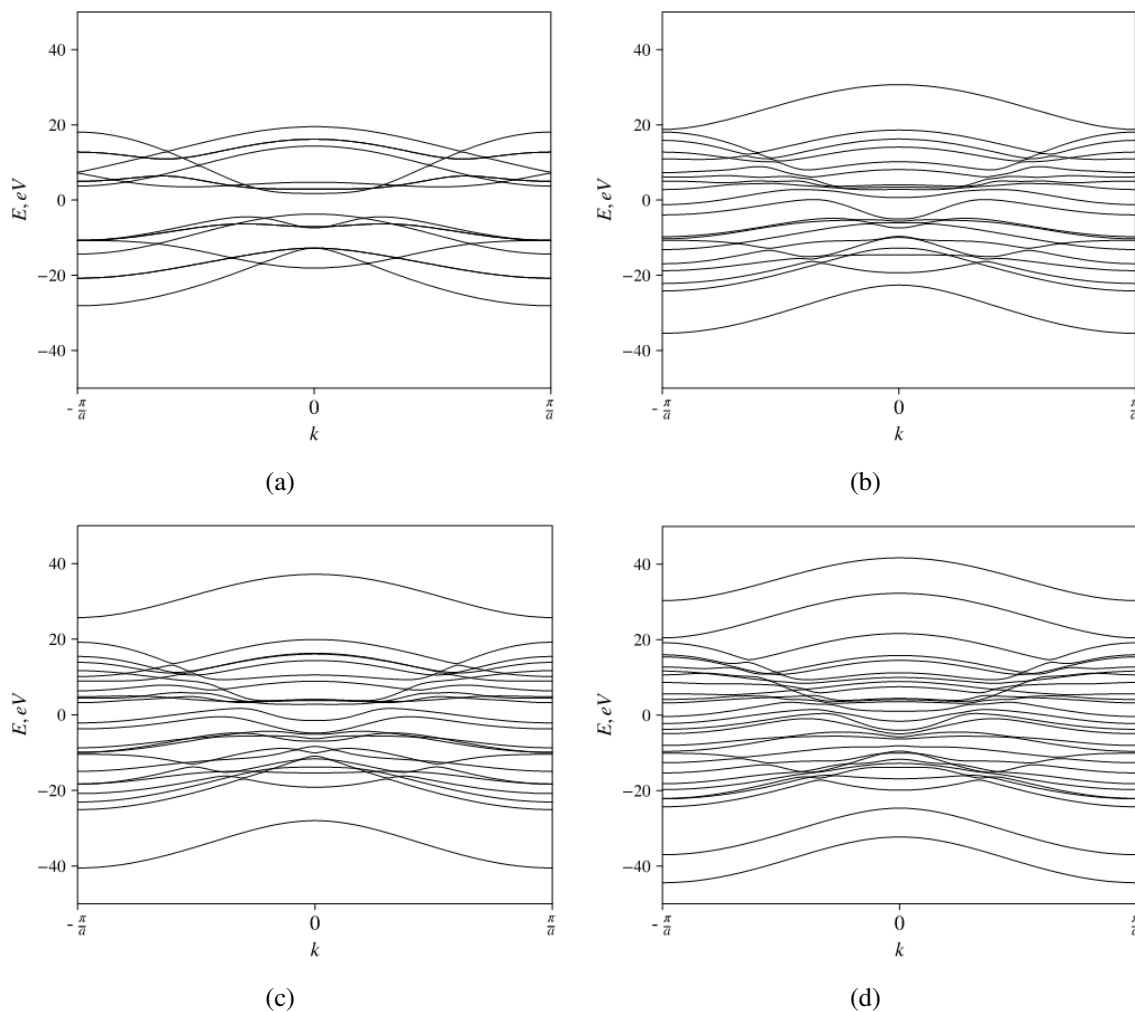


FIG. 3. Band structures of  $[n, 4]$  (a),  $[n, 5]$  (b),  $[n, 6]$  (c), and  $[n, 7]$  (d) CPPs at  $n \rightarrow \infty$

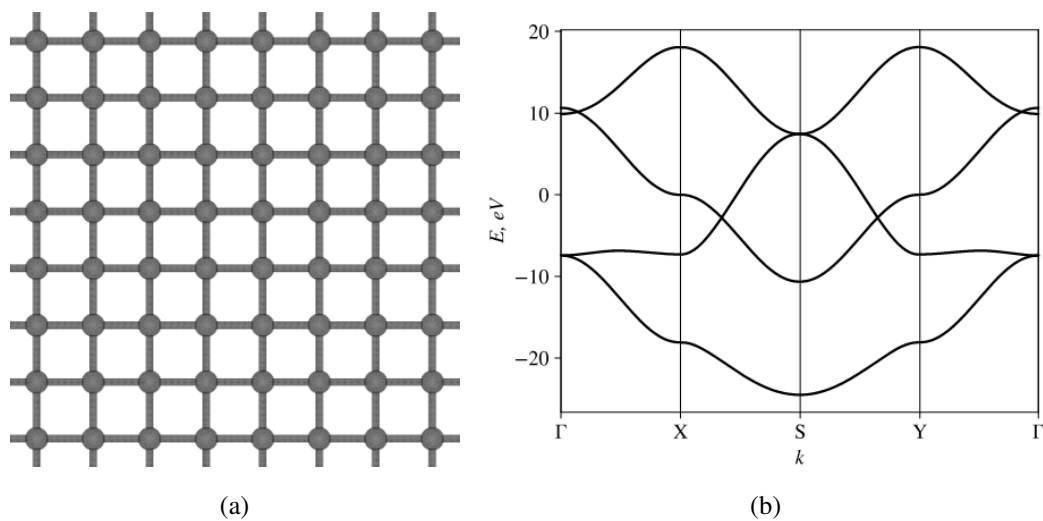


FIG. 4. A hypothetical infinite 2D square carbon lattice (a) and its band structure (b)

#### 4. Conclusion

In this paper, we applied the  $sp^3$ -TBM to study the electronic properties of long  $C_{[n,4]}$ ,  $C_{[n,5]}$ ,  $C_{[n,6]}$ , and  $C_{[n,7]}$  prismanes. Our findings show that  $C_{[n,4]}$  prismanes ( $n \rightarrow \infty$ ) feature relatively wide ( $\sim 2 - 10$  eV) band gaps and can be classified as semiconductors or dielectrics. Meanwhile, long  $C_{[n,m]}$  prismanes with  $m \geq 7$  (including  $m \rightarrow \infty$ ) possess no band gap at all, thus acting as good electrical conductors. Large variations in the  $sp^3$ -TBM parameter values do not have a qualitative effect on these results. We also found that long  $[n, 5]$  and  $[n, 6]$  CPPs can exhibit metallic, quasi-metallic, or semiconductor properties depending on the choice of these parameter values. Therefore, the electronic features of  $C_{[n,4]}$  and  $C_{[n,m]}$  prismanes at  $m \geq 7$  and  $n \rightarrow \infty$  are governed primarily by their topology rather than by the specific nature of carbon. We predict that similar behavior will occur in polyprismanes of other chemical elements (e.g., silicon and germanium). The demonstrated electronic transport properties of CPPs open fresh avenues for exploiting these carbon nanostructures as sub-nanometer wires and in other nanoelectronic device components.

#### References

- [1] Peng R., Pan Y., Liu B., Li Z., Pan P., Zhang S., Qin Z., Wheeler A., Tang X., Liu X. Understanding Carbon Nanotube-Based Ionic Diodes: Design and Mechanism. *Small*, 2021, **17** (31), 2100383.
- [2] Liang X., Li H., Dou J., Wang Q., He W., Wang C., Li D., Lin J.-M., Zhang Y. Stable and Biocompatible Carbon Nanotube Ink Mediated by Silk Protein for Printed Electronics. *Advanced Materials*, 2020, **32** (31), 2000165.
- [3] Cao Q. Carbon nanotube transistor technology for More-Moore scaling. *Nano Research*, 2021, **14** (9), 3051.
- [4] Shi H., Ding L., Zhong D., Han J., Liu L., Xu L., Sun P., Wang H., Zhou J., Fang L., Zhang Z., Peng L.-M. Radiofrequency transistors based on aligned carbon nanotube arrays. *Nature Electronics*, 2021, **4** (6), 405.
- [5] Lin Y., Liang S., Xu L., Liu L., Hu Q., Fan C., Liu Y., Han J., Zhang Z., Peng L.-M. Enhancement-Mode Field-Effect Transistors and High-Speed Integrated Circuits Based on Aligned Carbon Nanotube Films. *Advanced Functional Materials*, 2021, **32** (11), 2104539.
- [6] Franklin A.D., Hersam M.C., Wong P.H.-S. Carbon nanotube transistors: Making electronics from molecules. *Science*, 2020, **378** (6621), 726.
- [7] Lin Y., Cao Y., Ding S., Zhang P., Xu L., Liu C., Hu Q., Jin C., Peng L.-M., Zhang Z. Scaling aligned carbon nanotube transistors to a sub-10 nm node. *Nature Electronics*, 2023, **6**, 506.
- [8] Wan H., Cao Y., Lo L.-W., Zhao J., Sepulveda N., Wang C. Flexible Carbon Nanotube Synaptic Transistor for Neurological Electronic Skin Applications. *ACS Nano*, 2020, **14** (8), 10402.
- [9] Wang Z.-X., Du P.-Y., Li W.-J., Meng J.-H., Zhao L.-H., Jia S.-L., Jia L.-C. Highly rapid-response electrical heaters based on polymer-infiltrated carbon nanotube networks for battery thermal management at subzero temperatures. *Composites Science and Technology*, 2023, **231**, 109796.
- [10] Li Z., Shen C., Liu Y., Ma C., Li F., Yang B., Huang M., Wang Z., Dong L., Wolfgang S. Carbon Nanotube Filter Functionalized with Iron Oxide for Flow-through Electro-Fenton. *Applied Catalysis B: Environmental*, 2020, **260**, 118204.
- [11] Katin K.P., Shostachenko S.A., Avkhadiyeva A.I., Maslov M.M. Geometry, Energy, and Some Electronic Properties of Carbon Polyprismanes: Ab Initio and Tight-Binding Study. *Advances in Physical Chemistry*, 2015, **2015**, 506894.
- [12] Katz T.J., Acton N. Synthesis of prismane. *J. of the American Chemical Society*, 1973, **95** (8), 2738.
- [13] Eaton P.E., Cole T.W. The Cubane System. *J. of the American Chemical Society*, 1964, **86** (5), 962.
- [14] Eaton P.E., Or Y.S., Branca S.J. Pentaprismane. *J. of the American Chemical Society*, 1981, **103** (8), 2134.
- [15] Su S.-K., Chen E., Hung T.Y. T., Li M.-Z., Pitner G., Cheng C.-C., Wang H., Cai J., Wong H.-S.P., Radu I.P. Perspective on Low-dimensional Channel Materials for Extremely Scaled CMOS. *2022 IEEE Symposium on VLSI Technology and Circuits (VLSI Technology and Circuits)*. Honolulu, HI, USA, 12 – 17 June 2022, IEEE, 2022, P. 403.
- [16] Qiu C., Zhang Z., Xiao M., Yang Y., Zhong D., Peng L.-M. Scaling carbon nanotube complementary transistors to 5-nm gate lengths. *Science*, 2017, **355** (6322), 271.
- [17] Autreto P.A.S., Legoas S.B., Flores M.Z.S., Galvao D.S. Carbon nanotube with square cross-section: An ab initio investigation. *The Journal of Chemical Physics*, 2010, **133** (12), 124513.
- [18] Ohno K., Satoh H., Iwamoto T., Tokoyama H., Yamakado H. Exploration of Carbon Allotropes with Four-membered Ring Structures on Quantum Chemical Potential Energy Surfaces. *J. of Computational Chemistry*, 2018, **40** (1), 14.
- [19] Lewars E.G. *Modeling Marvels: Computational Anticipation of Novel Molecules*, Springer Science+Business Media, Luxembourg, 2008, P. 187–192.
- [20] Shostachenko S.A., Maslov M.M., Prudkovskiy V.S., Katin K.P. Thermal stability of hexaprismane  $C_{12}H_{12}$  and octaprismane  $C_{16}H_{16}$ . *Physics of the Solid State*, 2015, **57** (5), 1023.
- [21] Sergeev D. One-dimensional Schottky nanodiode based on telescoping polyprismanes. *Advances in Nano Research*, 2021, **10** (4), 339.
- [22] Baimova J.A., Rysaeva L.K., Rudskoy A.I. Deformation behavior of diamond-like phases: Molecular dynamics simulation. *Diamond and Related Materials*, 2017, **81**, 154.
- [23] Rysaeva L.K., Lisovenko D.S., Gorodtsov V.A., Baimova J.A. Stability, elastic properties and deformation behavior of graphene-based diamond-like phases. *Computational Materials Science*, 2019, **172**, 109355.
- [24] Baimova J.A., Galiakhmetova L.K., Mulyukov R. R. Diamond-like structures under hydrostatic loading: Atomistic simulation. *Computational Materials Science*, 2021, **192**, 110301.
- [25] Lyakhov A.O., Oganov A.R. Evolutionary search for superhard materials: Methodology and applications to forms of carbon and TiO. *Physical Review B*, 2011, **84** (9), 092103.
- [26] Kohn E., Denisenko A. Concepts for diamond electronics. *Thin Solid Films*, 2007, **515** (10), 4333.
- [27] Belenkov E.A., Greshnyakov V.A. Diamond-like phases prepared from graphene layers. *Physics of the Solid State*, 2015, **57** (1), 205.
- [28] Novikov N.V., Maslov M.M., Katin K.P., Prudkovskiy V.S. Effect of DFT-functional on the energy and electronic characteristics of carbon compounds with the unconventional geometry of the framework. *Letters on Materials*, 2017, **7** (4), 433.
- [29] Maslov M.M., Grishakov K.S., Gimaldinova M.A., Katin K.P. Carbon vs silicon polyprismanes: a comparative study of metallic  $sp^3$ -hybridized allotropes. *Fullerenes, Nanotubes and Carbon Nanostructures*, 2019, **28** (2), 97.
- [30] Gimaldinova M.A., Katin K.P., Salem M.A., Maslov M.M. Energy and electronic characteristics of silicon polyprismanes: Density functional theory study. *Letters on Materials*, 2018, **8** (4), 454.

- [31] Katin K.P., Grishakov K.S., Gimaldinova M.A., Maslov M.M. Silicon rebirth: Ab initio prediction of metallic  $sp^3$ -hybridized silicon allotropes. *Computational Materials Science*, 2020, **174**, 109480.
- [32] Merinov V.B., Khrushkova A.A. Ab initio prediction of metallic nature of  $sp^3$ -hybridized germanium structures. *Computational and Theoretical Chemistry*, 2024, **1231**, 114441.
- [33] Gaur A., Srivastava J. A tight-binding study of the electron transport through single-walled carbon nanotube-graphene hybrid nanostructures. *J. of Chemical Physics*, 2021, **155** (24), 244104.
- [34] Xin B., Zou K., Liu D., Li B., Dong H., Cheng Y., Liu H., Zou L.-J., Luo F., Lu F., Wang W.-H. Electronic structures and quantum capacitance of twisted bilayer graphene with defects based on three-band tight-binding model. *Physical Chemistry Chemical Physics*, 2024, **26** (12), 9687.
- [35] Mostafaei A., Semirovi E.H. A tight-binding model for the electronic structure of MXene monolayers. *Nanoscale*, 2022, **14**, 11760.
- [36] Peng Z., Guan Z., Wang H., Srolovitz D.J., Lei D. Modified tight-binding model for strain effects in monolayer transition metal dichalcogenides. *Physical Review B*, 2024, **109**, 245412.
- [37] Candioto G. Exploring the electronic potential of effective tight-binding Hamiltonians. *Materials Today Quantum*, 2024, **1**, 100001.
- [38] Slater J.C., Koster G.F. Simplified LCAO Method for the Periodic Potential Problem. *Physical Review*, 1954, **94** (6), P. 1498–1524.
- [39] Charlier J.-C., Lambin Ph., Ebbesen T.W. Electronic properties of carbon nanotubes with polygonized cross sections. *Physical Review B*, 1996, **54** (12), R8377–R8380.
- [40] Dag S., Senger R.T., Ciraci S. Theoretical study of crossed and parallel carbon nanotube junctions and three-dimensional grid structures. *Physical Review B*, 2004, **70** (20), 205407.
- [41] Wei-Yang Lo, George Y.-S. Wu, Kuei-Ching Wu. Tight-binding calculation with up to the 3rd nearest “neighbor” coupling for small-radius carbon nanotubes. *Physica E: Low-dimensional Systems and Nanostructures*, 2010, **43** (1), P. 482–486.
- [42] Kulbachinsky V.A. *Physics of nanosystems*. Phymathlit, Moscow, 2023, P. 513–515.
- [43] Schattauer C., Todorovic M., Ghosh K., Rinke P., Libisch F. Machine learning sparse tight-binding parameters for defects. *NPJ Computational Materials*, 2022, **8**, 116.
- [44] Nakhaee M., Ketabi S.A., Peeters F.M. Tight-Binding Studio: A technical software package to find the parameters of tight-binding Hamiltonian. *Computer Physics Communications*, 2020, **254**, 107379.
- [45] Zhang G., Musgrave C.B. Comparison of DFT Methods for Molecular Orbital Eigenvalue Calculations. *J. of Physical Chemistry A*, 2007, **111** (8), 1554.
- [46] Krylova K.A., Baimova Y.A., Dmitriev S.V., Mulyukov R.R. Calculation of the structure of carbon clusters based on fullerene-like  $C_{24}$  and  $C_{48}$  molecules. *Physics of the Solid State*, 2016, **58** (2), 394.

---

Submitted 10 March 2025; revised 5 April 2025; accepted 6 April 2025

#### Information about the authors:

Vladimir A. Kurakin – National Research Nuclear University MEPhI (Moscow Engineering Physics Institute), 31 Kashirskoe Hwy, Moscow 115409, Russian Federation; ORCID 0009-0001-1358-3685; fromkurakin@mail.ru

Tatyana N. Kobernik – Energy Technology Center, Skolkovo Institute of Science and Technology, Territory of Innovation Center “Skolkovo”, 30 (bld 1) Bolshoy Blvd, Moscow 121205, Russian Federation; ORCID 0009-0003-0223-9111; kobernik-t-n@yandex.ru

*Conflict of interest:* the authors declare no conflict of interest.